Proceedings of the 4th International Conference on Fluid Flow and Thermal Science (ICFFTS'23)
Lisbon, Portugal- December 07 - 09, 2023
Paper No. 169
DOI: 10.11159/icffts23.169

A Study Of Subcooled Pool Boiling Using Direct Numerical Simulations

Sara Youssoufi[1], Aaron Lentner[1], Amir Riaz[2], Elias Balaras[1]
[1]George Washington University/Department of Mechanical and Aerospace
Science & Engineering Hall, 800 22nd St NW, Washington, D.C, USA
sarayoussoufi@gwu.edu; balaras@gwu.edu
[2]University of Maryland/Department of Mechanical Engineering
Glenn L. Martin Hall, College Park, MD, USA
ariaz@umd.edu

Abstract – The impact of pool subcooling on nucleate boiling remains limited. Overall, in engineering applications it is assumed to have a negligible effect, although it is conjectured that there is potential for a shift in the boiling curve due to subcooling degree. The present work examines the effect of subcooled pool boiling on both heat flux and bubble dynamics by conducting detailed interface resolving direct numerical simulations (DNS). An in-house solver is used to solve the Navier Stokes equations for incompressible flow coupled to mass, momentum, and energy equations. A single fluid with variable properties approach is adapted where the interface between the liquid and vapor phases is tracked by the level set technique. Ghost fluid formulation is considered to account for sharp jumps in pressure, velocity, and temperature across multiphase boundaries. Two set of computations have been conducted. In the first set, bulk liquid temperature was varied while all other parameters were maintained constant. In the second set, Stefan's number was held constant. All cases show that subcooled pool boiling has an impact to the boiling curve and bubble dynamics. Computational results were compared to available empirical correlations. Variation of Stefan number revealed negligible effects. Furthermore, subcooling was observed to impact coherent vortices further way from the wall.

Keywords**:** Pool boiling, subcooling, superheat, bubble dynamics, heat flux

1. Introduction

The thermal design of systems play a significant role in managing heat transfer in different engineering applications; for example: nuclear reactors, spacecraft, aviation, and energy resources. Due to their surrounding environments, thermal systems are susceptible to overheat; as a result, industries and research have been looking for solutions. One of the possible heat transfer techniques is pool boiling. The different regimes of pool boiling can be identified in the "Nukiyama" curve (Figure 1c), which depicts the variation of wall heat flux with wall superheat temperature in a saturated pool of water at atmospheric pressure. The superheat is defined as the difference between wall temperature and saturation temperature. The pool system is called "subcooled" when the bulk liquid temperature is maintained at a temperature lower than the saturation temperature of the fluid, while it is called "saturated" when these two temperatures are equal. Over the years many parameters that influence the nucleate boiling regime, such as material roughness [3], wettability [4], surface enhancement [5], heater size [3], nucleation sites density [6], waiting time [7], thermal boundary layer [7], microlayer evaporation [8, 9], surface tension [10], contact angle [11], and gravitational force [12] have been explored. However, in engineering applications pool subcooling is generally considered to have a negligible effect on wall heat flux in the nucleate boiling regime, and only a linear effect on maximum and minimum heat fluxes [1].

Rohsenow [13], for example, demonstrates the negligible effect of subcooling based on experimental results and sugested that the wall heatflux is a power of the wall superheat, ΔT_{sup}^3. The results of Wang and Dhir [4], and Gaertner [14] both follow Rohsnow's power law relationship, while the work of Son and Dhir [6] obtained better agreement with the correlations of Stephan and Abdelsalam [15], where the heat flux varies as ΔT_{sup}. Linehard [16] studies Yamagata and Tien correlations [17] highlighting that both neglect the subcooling temperature effect. Monde and Katto [18] conclude that wall heat flux is driven only by wall superheat temperature. Moreover, available quality heat flux correlations generally do not include an effect of pool subcooling: for example Zuber and Zuber-Forster [9, 19], and Forster-Grief [9].

On the other hand, many studies emphasize the influence of pool subcooling on bubble dynamics, which is clearly important to the magnitude of wall heat flux in the nucleate boiling regime. Gunther and Kreith [20] observe that increased

subcooling degree delays or prevents bubble detachment. Ibrahim and Judd [21] report an inversion in the bubble growth time and bubble waiting time after reaching a subcooling degree equal to 6℃. Osu and Kunugi [22] investigate numerically subcooled pool boiling and notice two main effects when the subcooling degree is increased: the enhancement of the condensation rate and the reduction of the evaporation. However, the work of Kim et al. [23, 24, 25] observe a higher heat flux in subcooled pool boiling as compared to saturated pool boiling. They conclude that heat flux in subcooled pool boiling is affected by the buoyancy force through the bubble departure rate. They also found that superheat degree does not impact the distribution of bubble diameters. Mudawar and Anderson [5] also observed that the subcooling degree has an impact on reducing the size of the bubble.

A generally applicable, mechanistic theory of boiling is still to be developed [26]; in support of this task, exact mechanisms of influence of pool subcooling are not sufficiently detailed. The work presented in this paper aims to provide numerically derived subcooled pool boiling data, relate bubble motions to wall heat flux, and to quantitatively investigate the effect of saturation temperature and Stefan number. For this purpose a series of interface-solving, Direct Numerical Simulations (DNS) have been conducted. In the next section the details on the methodology and the parameteric space are given. Section 3 presents results on the wall het flux and bubble dynamics, followed by the concluding remarks.

2. Problem formulation and methodology

We consider nucleate boiling heat transfer over a micro-heater array placed inside a boiling chamber as in the experiments conducted by Kim et al. [24]. The equations governing the dynamics of the liquid and vapor phases are as follows:

$$\frac{\partial \vec{u}}{\partial t} + \vec{u} \cdot \nabla \vec{u} = -\frac{1}{\rho'} \nabla \mathrm{P} + \nabla \cdot \left[\frac{\mu'}{\rho'} \frac{1}{Re} \nabla \vec{u} \right] + \frac{1}{Fr^2} \tag{1a}$$

$$\frac{\partial \mathrm{T}}{\partial \mathrm{t}} + \vec{u} \cdot \nabla \mathrm{T} = \nabla \cdot \left[\frac{\alpha'}{Re\, Pr} \nabla T \right] \tag{1b}$$

where, $\vec{u}$, is the velocity, P is the pressure, and T is the temperature. The equations are non-dimensionalized with reference quantities from the liquid phase defining the Reynolds number, $Re = \rho_l u_0 l_0 / \mu_l$, Prandtl number, $\mathrm{Pr} = \mu_l C_{pl} / k_l$, and Froude number, $Fr = u_0 / \sqrt{g l_0}$, where u_0 and l_0 are the characteristic velocity and length scale respectively, that will be defined later. The normalized temperature is defined as, $T_i^* = (T_i - T_{wall})/(T_{wall} - T_{bulk})$, where T_i^* is the temperature at point i, T_{wall} is the wall/heater temperature and T_{bulk} is the bulk liquid temperature. Note that for the vapor phase, $\rho' = \rho_v / \rho_l$, $\mu' = \mu_v / \mu_l$, and $\alpha' = \alpha_v / \alpha_l$, and for the liquid phase, $\rho' = \mu' = \alpha' = 1$ (subscripts l and v refer to the liquid and vapor phases respectively, ρ refers to density, μ refers to thermal viscosity, and α refers to thermal diffusivity). The equation for conservation of mass can be written as:

$$\nabla \cdot \vec{u} = -\dot{m} \nabla \frac{1}{\rho'}|_{\Gamma} \cdot \vec{n} \tag{2}$$

$$\dot{m} = \frac{St}{Re\, Pr} [\nabla T_l|_{\Gamma} \cdot \vec{n} - k' \nabla T_v|_{\Gamma} \cdot \vec{n}] \tag{3}$$

where $\vec{n}$ is a unit vector normal to the interface, and $\dot{m}$ is the mass transfer calculated using Equation (3), $k' = k_v / k_l$ is the thermal conductivity and $St = C_{pl} \Delta T / h_{lv}$ is the Stefan number ($\Delta T = T_{wall} - T_{bulk}$ and h_{lv} is the latent heat of vaporization). The heat flux from the liquid region, ∇T_l, contributes towards evaporation, and the heat flux from vapor region, ∇T_v, accounts for condensation. The above system of equations is solved using an in-house solver [2]. The solver utilizes a single-fluid approach with variable fluid properties, and explicitly tracks the interface, Γ, between the liquid and vapor phases via a level-set formulation. A cartesian grid with a staggered arrangement of the flow variables is adopted and all spatial

derivatives are approximated with second-order finite-differences. For the time advancement a projection method is used, where all terms are advanced explicitly using an Adams-Bashforth scheme. At the liquid-vapor interface, Γ, boundary conditions for the velocity, pressure and temperature are enforced using a variant of the Ghost Fluid Method (GFM) [27]:

$$[P]_\Gamma = P_v - P_l = \frac{\kappa}{We} - \left(\frac{1}{\rho'} - 1\right)\dot{m}^2 \tag{4a}$$

$$[\vec{u}]_\Gamma = \vec{\boldsymbol{u}}_{\boldsymbol{v}} - \vec{\boldsymbol{u}}_{\boldsymbol{l}} = \dot{\boldsymbol{m}}\left(\frac{\mathbf{1}}{\boldsymbol{\rho'}} - \mathbf{1}\right)\vec{\boldsymbol{n}} \tag{4b}$$

$$T_\Gamma = T_{sat} \tag{4c}$$

where, κ, is the interface curvature, $We = \rho_l u_0^2 l_0/\sigma$ is the Weber number, and T_{sat}, is the saturation temperature. The details of our implementation together with an extensive validation for a variety of pool boiling problems of increasing complexity can be found in Dhruv et al. [28]. The adopted computational domain is shown in Figure 1a and it is designed to mimic the experiments by Kim et al. [24]. In the later, a micro-heater comprised of 96 platinum resistance heaters in a 10×10 configuration arrangement is used. Each heater in the array has the size of $0.7\ mm \times 0.7\ mm$, which results in a total heated area of $7\ mm \times 7\ mm$. The micro-heater arrays are placed inside a chamber of size $288\ mm \times 144\ mm \times 144\ mm$. In Figure 1a all lengths are normalized by a reference length scale $l_0 = \sqrt{\sigma/(\rho_l - \rho_v)g}$, which is $l_0 = 0.7\ mm$, corresponding to the capillary length, L_c^g, in earth gravity, $g = 9.8\ m/s^2$. The corresponding velocity reference scale is defined as $u_0 = \sqrt{g l_0}$.

On the heated surface, a no-slip boundary condition is enforced for the velocity field and a Dirichlet boundary condition is used for the temperature ($T = T_{wall}$). At the top of the computational domain, homogeneous Neumann boundary condition ($\partial v/\partial n = 0$) is applied to the velocity, while Dirichlet boundary conditions are used for the pressure ($P = 0$) and temperature ($T = T_{bulk}$). The remaining portions of the computational domain along the sides are modelled as adiabatic slip walls. The working fluid in all cases is FC-72 where the values of physical parameters are listed in Table 1.

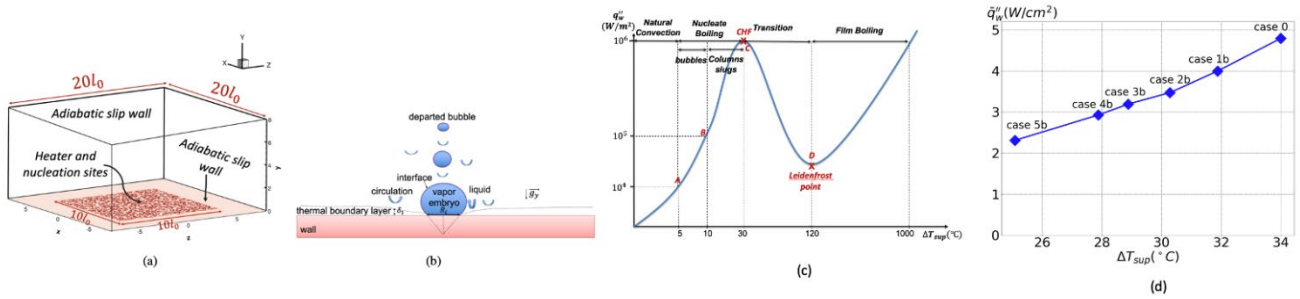

Fig. 1: (a) Computational domain for the pool boiling problem highlighting heater (red) and nucleation sites (blue); (b) Schematic of a bubble forming at a nucleation site, (c) Nukiyama boiling curve, (d) Boiling curve related to the studied cases.

Table 1: Dimensional physical parameters for FC-72 fluid.

Parameters	ρ_l	ρ_v	C_{pl}	C_{pv}	h_{lv}	μ_l	μ_v	k_l	k_v	σ
Values	1620	13.5	1110	925	83562	$4e^{-4}$	$4e^{-4}$	$5.4e^{-2}$	$1.35e^{-2}$	$8.3e^{-3}$
Units	kg/m^3	kg/m^3	J/kgK	J/kgK	J/kg	Ns/m^2	Ns/m^2	W/mK	W/mK	N/m

In the first set of computations (cases 0 to 3) the heater temperature is kept constant at $T_{wall} = 92$°C , the saturation temperature is set at $T_{sat} = 58$°C, while the bulk temperature was varied to investigate the effect of different levels of pool subcooling (ΔT_{sub}) while maintaining the superheat constant (ΔT_{sup}). The wall superheat and subcooling are defined as, $\Delta T_{sup} = 34$°C and 5°C $< \Delta T_{sub} < 13$°C. Note that the case of $\Delta T_{sub} = 8$°C matches the conditions in the experiments by

Kim et al. [24]. Additional set of computations (cases 1b to 5b) are conducted to investigate the effect of Stefan number and superheat temperature. Stefan number was fixed to 0.5298 corresponding to the reference simulation. Table 2 summarizes dimensional and non-dimensional parameters. Non dimensional parameters noted with an asterisk $(*)$.

Table 2: Non-dimensional and dimensional overview of carried computational cases.

Cases	T^*_{sat}	St^*	ΔT^*_{sub}	ΔT^*_{sup}	T_{bulk}(℃)	T_{wall}(℃)	ΔT_{sub}(℃)
saturated	0	0.5298	0	34	58	92	0
case 0	0.128	0.4516	5	34	53	92.88	5
case 1	0.1904	0.5579	8	34	50	92	8
case 2	0.2444	0.5978	11	34	47	92	11
case 3	0.2766	0.6243	13	34	45	92	13
case 1b	0.1904	0.5298	7.47	31.88	50.52	89.88	7.48
case 2b	0.2444	0.5298	9.56	30.28	48.43	88.28	9.57
case 3b	0.2766	0.5298	10.68	28.88	47.31	86.88	10.69
case 4b	0.306	0.5298	11.95	27.88	46.04	85.88	11.96
case 5b	0.370	0.5298	14.73	25.08	43.26	83.03	14.74

Furthermore, to fully define the problem, nucleation sites on the heater must be specified. Although details on this multi-scale process are not well understood, it is generally accepted that the surface topography and wall superheat play an important role as discussed in [29]. In this work, we consider smooth wall (roughness is not resolved) and specified nucleation sites using a Halton sequence [30]. The input to this algorithm is the nucleation site density, which was extracted from the experimental results [24]. Particularly, for a superheat of $\Delta T_{sup} = 34$℃, we estimated a bubble density of the $6\ bubbles/mm^2$, resulting to a total of $600\ bubbles$ on the heater. In each site, when necessary, bubble embryos with a diameter of a 2-3 local grid cells were introduced and start to grow dynamically by evaporation based on the local flow conditions (see Figure 1b). The details on the overall algorithm can be found in [12].

3. Results

3.1. Overview

The temporal variation of the total overall heat flux q''^*_w at the wall is reported in Figure 2. All simulations started from the same initial conditions and reached the quasi-steady state after 10 computational time units. The transient period seems to be independent of subcooling and superheat. The value t^* is given as $t(s)/t_0$, where t_0 is the reference time scale calculated using expressions of l_0 and u_0 $(t_0 = 8s)$. Cases 1/1b, 2/2b, and 3/3b show that Stefan number has negligible impact on heat flux. Figure 2 illustrates the effect of subcooling on heat flux: the average of total heat flux decreases by 21.95% from case 0 to case 3, and by 34.67% from case 0 to case 5b. It is also clear that an increase of the wall superheat from $\Delta T_{sup} = 25.08$ in case 5b, to $\Delta T_{sup} = 34$ in case 0 leads to an increase in wall heat flux by 34.67%. Furthermore, according to visual observations of bubble dynamics, a slight increase of wall superheat, for example from case 2b to case 1b or from case 3b to case 2b activates many rising bubbles. Heat flux is therefore sensitive to superheat and subcooling degrees. The more subcooling degree increases, the less bubble departure occurred (Figure 5), and the less heat flux is obtained (Figure 2). These observations agree with Zuber and Jakob [31] who constate that an increase in heat flux in nucleate boiling is always accompanied by an increase in bubble departures; the later create fluid agitation at the near wall and participate in return in increasing the heat flux. The absence of bubble detachments in high subcooling is also in agreement with Gunther and Kreith [20]. Concerning the saturated pool boiling, the curve of the heat flux is observed to be higher than all subcooled cases (figure 2a), which disagrees Kim et al. [23, 24] observations. This disagreement could be due to the difference in heater size, waiting time, and number of nucleation sites since their results are based on experiments inducing a variation in all these parameters, while our results are based

on computational model with fixed waiting time and nucleation sites and different heater size than what was used in [23, 24].

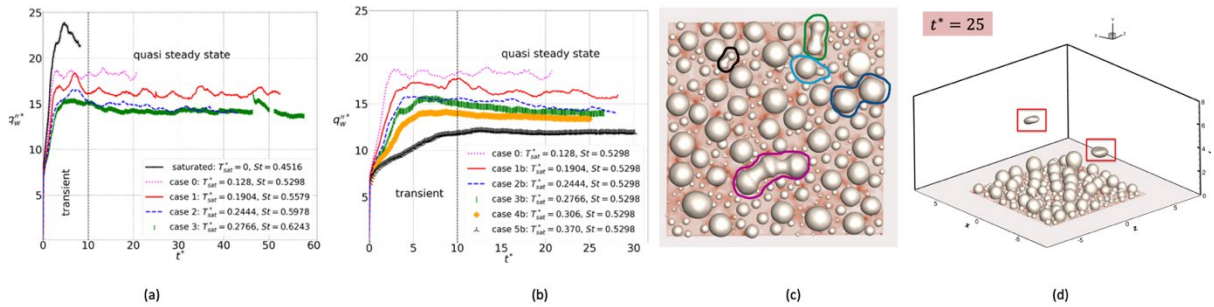

Fig. 2: (a, b) Temporal variation of total wall heat flux for saturated and subcooled pool boiling cases, (c) illustration of bubble merger dynamics, (d) illustration of bubble departure dynamics

3.1. Heat Flux analysis

A comparion of the averaged heat flux obtained from the simulations gainst existent heat flux correlations for pool boiling is presented in Figure 3a-3b. Empirical correlations such as Yamagata [17], Tien [17], Zuber [9, 19], and Forster-Grief [9, 32] underestimate the heat flux, while Rohsenow [13] and Forster-Zuber [9, 19] overestimate the heat flux. Besides, using the same fluid conditions, each empirical correlation led to different heat flux results. These differences could be attributed to the effects of subcooling.

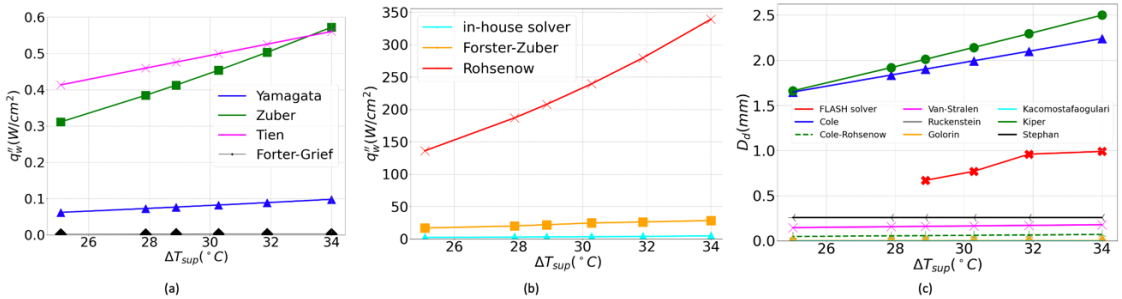

Fig. 3: (a), (b) Benchmark against existent pool boiling heat flux correlations, (c) Benchmark against departure diameter empirical correlations vs superheat temperature.

3.2. Bubble dynamic analysis

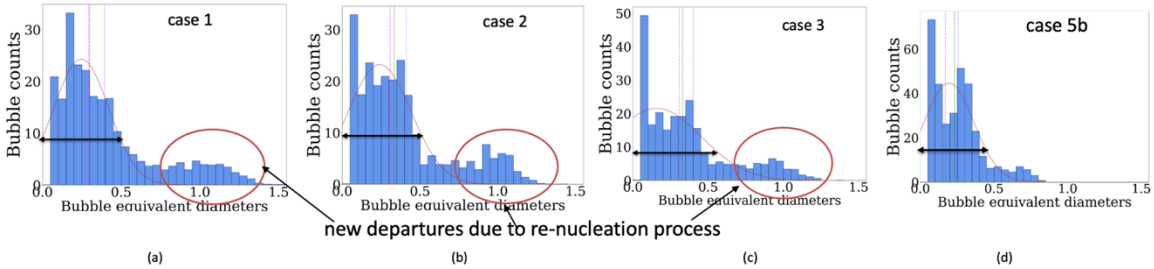

Fig. 4: Statistical distribution of bubble equivalent diameters for low, intermediate, and high subcooling

The mean bubble departure diameter, bubble departure frequency, bubble growth time, bubble waiting time, and nucleation site density are all part of the bubble dyanamics. In the present work, waiting time, and nucleation sites are the same in all

simulations. For the quantification of bubble dynamics we developed post-procesing tools based on the image processing python library scikit-image [41]. Figure 4 shows statistical distribution of bubble equivalent diameter for low, intermediate, and high subcooling. Similar trends were obtained for cases 1 and 1b, 2 and 2b and 3 and 3b which reinforce the fact that Stefan number has insignificant effect on bubble dynamics. The amplitude of the curves in Figure 4 becomes wider as subcooling degree increases (from case 1 to case 3, and from case 1b to case 5b). As the degree of subcooling increases, surface force becomes dominant, attracts bubbles to the heated surface, and competes against buoyancy force. As a result, the frequency of bubble departures decreases making the amplitude of the statistical distribution larger. Moreover, as subcooling degree increases, surface force increases as well, forcing bubbles to remain attached to the heater and provoking more coalescence and interactions between them. This explains the creation of a new population outside the red curve.

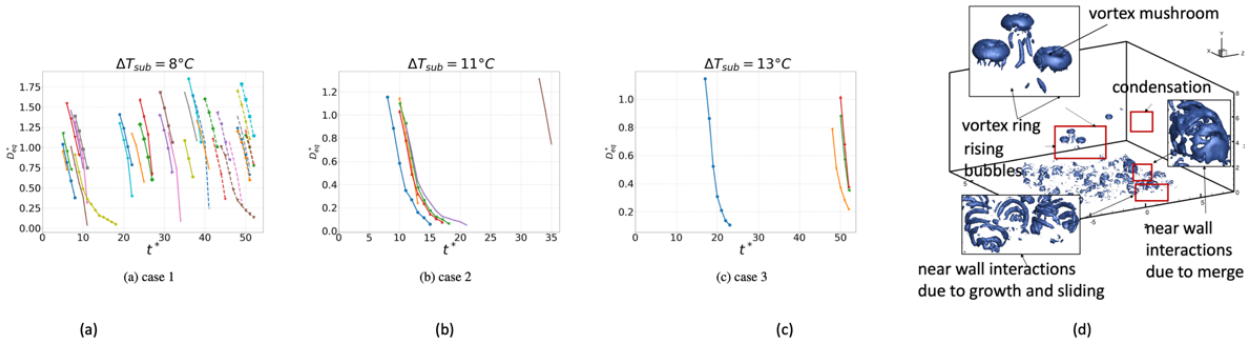

Fig. 5: (a), (b), (c) Evolution of bubble departure diameter in y-direction for all rising bubble, (d) Coherent vortices for case 2b, (e)coherent vortices for case 2b, (f) coherent vortices for case 4b.

Figure 5 shows the decrease of the departure diameters when rising bubbles go further from the wall. This is due to artificial condensation applied in the buffer region ($6 < y < 8$). The goal of the buffer region is to make bubbles avoid hitting the top surface of the boiling chamber. Note that Figure 5 does not account bubbles evolution in the buffer region which explain the linearity of the results. Bubble radius is seen to shrink as the subcooling increases since the surface tension force becomes stronger. The mean bubble departure diameter in the steady state period is $D_d = 0.9688\ mm$ for case 1, $D_d = 0.7771\ mm$ for case 2, and $D_d = 0.6711\ mm$ for case 3. Dimensional values were obtained using the conversion $D_d = D_d^* \times l_0$. Furthermore, coherent vortices are observed to have irregular patterns at near wall interactions, however further away from the wall, mushroom- likely vortices are dominant in low subcooling, ring vortices in intermediate subcooling and irregular patterns in high subcooling.

Obtained departure bubble diameters from the computational simulations was compared to empirical correlations: Cole [33], Cole and Rohsenow [34], Stralen [35], Ruckenstein [36], Golorin [37], Kocamustafaogullari [38], Kiper [39], and Stefan [40]. Results are reported in Figure 3c. Departure bubble diameters obtained from simulations are situated in the same range of departure bubble diameters predicted by the empirical correlations. The closest models are Stephan, Kiper, and Cole. However empirical correlations always predict departure diameters even when there are no rising bubbles (example case 4b and case 5b). This shows that additional parameters need to be reconsidered in establishing the empirical correlations of bubble departure diameters, such as subcooling degree, nucleation sites, and waiting time.

4. Conclusions

We have presented subcooled pool boiling hig-fidelity, interface resolvoing simulations. The main results in this work are the following: existent empirical correlations that predict bubble departure diameters agrees with the obtained results, however existent empirical heat flux correlations under-estimate the effect of subcooling. Careful investigations are needed in the future concerning the impact of waiting time (which is well demonstrated to impact numerical simulation of nucleate boiling on horizontal surfaces [7]) and nucleation sites to verify the presence of an effect of pool

subcooling of wall heat flux. Careful study is particularly important considering the observed effect contradicts accepted engineering practice.

Acknowledgements

The authors are grateful to National Aeronautics and Space Administration (NASA) who support this research under Grant no. NNX16AQ77G monitored by Dr. John MacQuillen. This research used NASA supercomputing environment to run CFD simulations with about a thousand cores for each simulation.

References

[1] Incropera, F.P., DeWitt, D.P., Bergman, T.L., Lavine, A.S., et al., 1996. Fundamentals of heat and mass transfer. Volume 6. Wiley New York

[2] Dhruv, A., 2020. A Multiphase Solver for High-Fidelity Phase-Change Simulations over Complex Geometries, Ph.D. Thesis, George Washington University.

[3] Rainey, K., You, S., 2001. Effects of heater size and orientation on pool boiling heat transfer from microporous coated surfaces. International Journal of Heat and Mass Transfer 44, 2589-2599.

[4] Wang, C., Dhir, V., 1993. Effect of surface wettability on active nucleation site density during pool boiling of water on a vertical surface.

[5] Mudawar, I., Anderson, T., 1990. Parametric investigation into the effects of pressure, subcooling, surface augmentation and choice of coolant on pool boiling in the design of cooling for high-power density electronic chips.

[6] Son, G., Dhir, V.K., 2008. Numerical simulation of nucleate boiling on a horizontal surface at high heat fluxes. International Journal of heat and Mass transfer 51, 2566-2582.

[7] Son, G., Dhir, V.K., Ramanujapu, N., 1999. Dynamics and heat transfer associated with a single bubble during nucleate boiling on a horizontal surface.

[8] Lee, R., Nydhal, J., 1989. Numerical calculation of bubble growth in nucleate boiling from inception through departure.

[9] Hameed, M.S., Khan, A.R., Mahdi, A., 2013. Modelling a general equation for pool boiling heat transfer. Advances in Chemical Engineering and Science 2013.

[10] Jontz, P., Myers, J., 1960. The effect of dynamic surface tension on nucleate boiling coefficients. AIChE Journal 6, 34-38.

[11] Mukherjee, A., Kandlikar, S.G., 2007. Numerical study of single bubbles with dynamic contact angle during nucleate pool boiling. International Journal of Heat and Mass Transfer 50, 127-138.

[12] Dhruv, A., Balaras, E.Riaz, A., Kim, J., 2021. An investigation of the gravity effects on pool boiling heat transfer via high-fidelity simulations. International Journal of Heat and Mass Transfer 180, 121826.

[13] Rohsenow, W.M., 1952. A method of correlating heat transfer data for surface boiling of liquids. Transactions of the American Society of Mechanical Engineers 74, 969-975.

[14] Gaertner, R.F., 1965, Photographic study of nucleate pool boiling on a horizontal surface.

[15] Stephan, K., Abdelsala, M., 1980. Heat-transfer correlations for natural convection boiling International Journal of Heat and Mass Transfer 23, 73-87

[16] Linehard, J., 1963. A semi-rational nucleate boiling heat flux correlation. International Journal of Heat and Mass Transfer 6, 215-219.

[17] Tien, C., 1962. A hydrodynamic model for nucleate pool boiling. International Journal of Heat and Mass Transfer 5, 533-540.

[18] Monde, M., Katto, Y., 1978. Burnout in a high heat-flux boiling system with an impinging jet. International Journal of Heat and Mass Transfer 21, 295-305.

[19] Passos, J., Reinaldo, R., 2000. Analysis of pool boiling within smooth and grooved tubes. Experimental Thermal and Fluid Science 22, 35-44.

[20] Gunther, F.C., Kreith, F., 1950. Photographic study of bubble formation in heat transfer to subcooled water. Jet Propulsion Laboratory Progress Report, 1-29.

[21] Ibrahim, E., Judd, R., 1985. An experimental investigation of the effect of subcooling on bubble growth and waiting time in nucleate boiling.
[22] Ose, Y., Kunugi, T., 2011. Numerical study on subcooled pool boiling, in: ASME/JSME Thermal Engineering Joint Conference, p. T10193.
[23] Kim, J., Benton, J.F., 2002. Highly subcooled pool boiling heat transfer at various gravity levels. International journal of heat and fluid flow 23, 497-508.
[24] Kim, J., Benton, J.F., Wisniewski, D., 2002. Pool boiling heat transfer on small heaters: effect of gravity and subcooling. International Journal of Heat and Mass Transfer 45, 3919-3932.
[25] Kim, J., Benton, J., Kucner, R., 2000. Subcooled Pool Boiling Heat Transfer Mechanisms inMicrogravity: Terrier-Improved Orion Sounding Rocket Experiment. Technical Report.
[26] Dhir, V.K., 2006. Mechanistic prediction of nucleate boiling heat transfer-achievable or a hopeless task?
[27] Kang, M., Fedkiw, R.P, Liu, X.D, 2000. A boundary condition capturing method for multiphase incompressible flow. Journal of Scientific Computing 15, 323-360.
[28] Dhruv, A., Balaras, E., Riaz, A., Kim, J., 2019. A formulation for high-fidelity simulations of pool boiling in low gravity. International Journal of Multiphase Flow 120, 103099.
[29] Zhang, L., Wang, T., Kim, S., Jiang, Y., 2020. The effects of wall superheat and surface wettability on nucleation site interactions during boiling. International Journal of Heat and Mass Transfer 146, 118820.
[30] Faure, H., Kritzer, P., Pillichshammer, F., 2015. From van der corput to modern constructions of sequences for quasi-monte carlo rules, Indagationes mathematicae 26, 760-822.
[31] Zuber, N., 1958. On the stability of boiling heat transfer. Transactions of the American Society of Mechanical Engineers 80, 711-714.
[32] Engelberg-Forster, K., Greif, R., 1959. Heat transfer to a boiling liquid – mechanism and correlations. Journal of Heat Transfer 81, 43-52.
[33] Cole, R., 1967. Bubble frequencies and departure volumes at subatmospheric pressures. AIChE Journal 13, 779-783.
[34] Cole, R., Rohsenow, W.M., 1969. Correlation of bubble departure diameters for boiling of saturated liquids, in: Chem. Eng. Prog. Symp. Ser, 2111213. Pp.211-213.
[35] Van Stralen, S., 1966. The mechanism of nucleate boiling in pure liquids and in binary mixtures- part i. International Journal of Heat and Mass Transfer 9, 995-1020.
[36] Ruckenstein, R., 1964. Recent trends in boiling heat transfer research. Appl.Mech.Rev 17, 663-672.
[37] Golorin, V., Kol'chugin, B., 1978. Investigation of the mechanism of nucleate boiling of ethyl alcohol and benzene by means of high-speed motion picture photography.
[38] Kocamustafaogullari, G., 1983. Pressure dependence of bubble departure diameter for water. International communications in heat and mass transfer 10, 501-509.
[39] Kiper, A., 1971. Minimum bubble departure diameter in nucleate pool boiling. International Joural of Heat and Mass Transfer 14, 931-937.
[40] Stefan, K., 1992. Saturated pool boiling and subcooled flow boiling of mixtures. University of Auckland, Newzland.
[41] Van der Walt, S., Schönberger, J.L., Nunez-Iglesias, J., Boulogne, F., Warner, J.D., Yager, N., Gouillard, E., Yu, T., 2014. Scikit-image: imageprocessing in python. PeerJ 2, e453.